# Signatures of octupole correlations in neutron-rich odd-mass barium isotopes

**Nomura, Kosuke; Nikšić, Tamara; Vretenar, Dario**

# Signatures of octupole correlations in neutron-rich odd-mass barium isotopes

K. Nomura, T. Nikšić, and D. Vretenar
*Physics Department, Faculty of Science, University of Zagreb, 10000 Zagreb, Croatia*

(Received 27 November 2017; revised manuscript received 18 January 2018; published 16 February 2018)

Octupole deformation and the relevant spectroscopic properties of neutron-rich odd-mass barium isotopes are investigated in a theoretical framework based on nuclear density functional theory and the particle-core coupling scheme. The interacting-boson Hamiltonian that describes the octupole-deformed even-even core nucleus, as well as the single-particle energies and occupation probabilities of an unpaired nucleon, are completely determined by microscopic axially symmetric $(\beta_2,\beta_3)$-deformation constrained self-consistent mean-field calculations for a specific choice of the energy density functional and pairing interaction. A boson-fermion interaction that involves both quadrupole and octupole degrees of freedom is introduced, and their strength parameters are determined to reproduce selected spectroscopic data for the odd-mass nuclei. The model reproduces recent experimental results for both even-even and odd-mass Ba isotopes. In particular, for $^{145,147}$Ba our results indicate, in agreement with recent data, that octupole deformation does not determine the structure of the lowest states in the vicinity of the ground state, and only becomes relevant at higher excitation energies.

DOI: 10.1103/PhysRevC.97.024317

## I. INTRODUCTION

Experiments using radioactive ion beams (RIBs) provide access to previously unknown short-lived nuclei far from the valley of $\beta$ stability. Among the most basic nuclear properties that have been extensively explored over many decades are geometrical shapes of nucleon density distributions and the corresponding excitation patterns. In particular, reflection-asymmetric octupole (or pear-shaped) deformation [1] has been a recurrent theme of interest in nuclear structure physics, from both the experimental and theoretical points of view. Atoms with octupole-deformed nuclei are particularly relevant in the context of the violation of time-reversal (T) invariance in the standard model of particle physics [2,3]. A number of new experiments are either running or being planned at major RIB facilities around the world. Recently, experimental evidence for permanent octupole deformation in radioactive nuclei has been reported, e.g., $^{224}$Ra and $^{220}$Rn at CERN [4] and $^{144}$Ba [5] and $^{146}$Ba [6] at Argonne National Laboratory.

Octupole deformation is also relevant for nuclei with odd nucleon numbers, particularly the interplay between single-particle degrees of freedom and the quadrupole and octupole collective degrees of freedom that determine the structure of low-lying states. Furthermore, in odd-$A$ octupole-deformed nuclei the Schiff moment, that is, a measure of nuclear time-reversal violation, is particularly enhanced. Examples are $^{225}$Ra [3,7] and $^{199}$Hg [8]. As a wealth of new data on odd-nucleon systems become accessible, timely and accurate theoretical studies of their spectroscopic properties are needed. From the computational point of view, however, a microscopic description of odd-mass nuclei is highly demanding, particularly in medium- and heavy-mass systems. The reason is partly because of the fact that in the odd-nucleon systems one must explicitly consider single-particle degrees of freedom, and treat them on the same level with collective degrees of freedom. Modeling the structure of odd-$A$ nuclei is even more complicated when octupole collective degrees of freedom are involved.

Recently we developed a novel method [9] for calculating spectroscopic properties of odd-mass nuclear systems, based on the framework of nuclear density functional theory and the particle-core coupling scheme. Our approach enables an accurate, systematic, and computationally feasible description of the odd-mass nuclei. The even-even core nucleus is described in the language of the interacting boson model (IBM) [10], and the particle-core coupling is taken from the interacting boson-fermion model (IBFM) [11]. The deformation energy surface for the even-even-core nucleus, the single-particle energies, and occupation probabilities of the unpaired nucleon are determined by a microscopic self-consistent mean-field (SCMF) calculation for a given energy density functional and pairing interaction. These mean-field results are then used as input for the IBFM Hamiltonian. However, several strength parameters of the boson-fermion interaction need to be specifically adjusted to reproduce selected data for the low-energy excitation spectra in the odd-mass nuclei.

In this work we extend the approach of Ref. [9] to a description of spectroscopic properties of odd-mass systems in which octupole deformation is expected to play a role. Here the major development of the method is that the boson-core Hamiltonian is not only built from the usual positive-parity $J^\pi = 0^+$ monopole ($s$) and $J^\pi = 2^+$ quadrupole ($d$) bosons, but also contains the negative-parity $J^\pi = 3^-$ octupole ($f$) boson. The $sdf$-IBM Hamiltonian is then determined by mapping the microscopic quadrupole-octupole deformation energy surface onto the expectation value of the Hamiltonian in the $sdf$ boson condensate state. The boson-fermion coupling Hamiltonian that includes both quadrupole and octupole boson degrees of freedom contains strength parameters adjusted to reproduce low-energy states in the odd-mass nucleus.

 

The present study is focused on spectroscopic properties of the neutron-rich odd-mass nuclei $^{143,145,147}$Ba. For the nucleus $^{145}$Ba, in particular, recent experiments suggest that there are no signatures of static octupole deformation in the ground- and low-lying states [12,13], even though the neighboring even-even nucleus $^{144}$Ba has long been considered as an example of pronounced octupole correlations [14]. Spectroscopic data are available in the neighboring even-even as well as odd-even Ba isotopes, and this experimental information allows us to constrain the strength parameters for the boson-fermion interaction in an unambiguous manner, even though the $sdf$-IBFM Hamiltonian contains more parameters than the simpler $sd$-IBFM.

In Ref. [15] the $sdf$-IBM framework, with the Hamiltonian determined from a $\beta_2\beta_3$-constrained SCMF calculation, has already been employed in a systematic study of quadrupole-octupole shape phase transitions in medium-heavy and heavy even-even nuclei [16]. Therefore, here we can utilize the mapped $sdf$-IBM Hamiltonian used in [16] for the description of the even-even $sdf$-boson core. It should be emphasized that IBFM calculations with an octupole-deformed boson core have rarely been pursued in the literature. To the best of our knowledge, it is only in the phenomenological studies of Refs. [17–19] that octupole bosons were explicitly included in the description of interacting boson-fermion systems.

In Sec. II we outline the method to analyze odd-mass systems with octupole degrees of freedom and briefly discuss the strength parameters of the particle-core coupling. Results for both the SCMF and the mapped $sdf$-IBM calculations for the even-even nuclei $^{142,144,146}$Ba are discussed in Sec. III. In Sec. IV we present results for the odd-mass nuclei $^{143,145,147}$Ba, including the systematics of low-energy positive- and negative-parity yrast states and detailed low-energy level schemes, as well as $E2$ and $E3$ transition rates in each odd-mass nucleus. A particular emphasis is put on the effect of octupole deformation in the low-lying states of odd-mass Ba nuclei. Finally, a short summary and outlook for future studies are included in Sec. V.

## II. MODEL

The starting point of the present analysis is to perform, for each even-even Ba nucleus, a self-consistent mean-field (SCMF) axially symmetric $(\beta_2,\beta_3)$ calculation with constraints on the mass quadrupole $Q_{20}$ and octupole $Q_{30}$ moments. The dimensionless shape variables $\beta_\lambda$ ($\lambda = 2,3$) are associated with the multipole moments $Q_{\lambda 0}$:

$$\beta_\lambda = \frac{4\pi}{3AR^\lambda} Q_{\lambda 0}, \tag{1}$$

with $R = 1.2A^{1/3}$ fm. The relativistic Hartree-Bogoliubov model [20] is used to calculate the $(\beta_2,\beta_3)$ deformation energy surface, single-particle energies, and particle occupation numbers, using the DD-PC1 functional [21] in the particle-hole channel, and a separable pairing force of finite range [22] in the particle-particle channel. These quantities are subsequently used as microscopic input for the phenomenological IBFM Hamiltonian.

TABLE I. Parameters of the $sdf$ IBM Hamiltonian. $\epsilon_d, \epsilon_f, \kappa_2, \kappa_3$, and $\alpha$ are in units of MeV, and the others are dimensionless.

| | $\epsilon_d$ | $\epsilon_f$ | $\kappa_2$ | $\chi_{dd}$ | $\chi_{ff}$ | $\alpha$ | $\kappa_3$ | $\chi_{df}$ |
|---|---|---|---|---|---|---|---|---|
| $^{142}$Ba | 0.412 | 0.958 | −0.100 | −1.2 | −1.90 | −0.0030 | 0.030 | −0.8 |
| $^{144}$Ba | 0.433 | 0.710 | −0.098 | −1.3 | −2.70 | −0.0199 | 0.048 | −1.5 |
| $^{146}$Ba | 0.202 | 0.729 | −0.098 | −1.2 | −2.75 | −0.0105 | 0.045 | −1.5 |

The IBFM Hamiltonian that describes the odd-mass system is composed of the boson-core Hamiltonian $\hat{H}_B$, the fermion Hamiltonian $\hat{H}_F$, and the Hamiltonian $\hat{H}_{BF}$ that couples the boson and fermion degrees of freedom:

$$\hat{H}_{\rm IBFM} = \hat{H}_B + \hat{H}_F + \hat{H}_{BF}. \tag{2}$$

The $sdf$-IBM Hamiltonian $\hat{H}_B$ of the quadrupole- and octupole-deformed even-even boson core nucleus reads

$$\begin{aligned}\hat{H}_B = {} & \epsilon_d \hat{n}_d + \epsilon_f \hat{n}_f + \kappa_2 \hat{Q}\cdot\hat{Q} \\ & + \alpha \hat{L}_d \cdot \hat{L}_d + \kappa_3 : \hat{V}_3^\dagger \cdot \hat{V}_3 :\end{aligned} \tag{3}$$

This form of the boson Hamiltonian has already been employed in Ref. [16], and it can be derived by projecting a fully symmetric state in the proton-neutron $sdf$ IBM-2 space onto the corresponding IBM-1 state [23]. The first and second terms in Eq. (3) are the $d$ and $f$ boson number operators, while the third term in the same equation is the quadrupole-quadrupole interaction with the quadrupole operator

$$\hat{Q} = s^\dagger \tilde{d} + d^\dagger \tilde{s} + \chi_{dd}[d^\dagger \times \tilde{d}]^{(2)} + \chi_{ff}[f^\dagger \times \tilde{f}]^{(2)}. \tag{4}$$

The fourth term in Eq. (3) denotes the rotational term with the angular momentum operator $\hat{L}_d = \sqrt{10}[d^\dagger \times \tilde{d}]^{(1)}$ and, finally, the last term is the octupole-octupole interaction written in the normal-ordered form with $\hat{V}_3^\dagger$ given by

$$\hat{V}_3^\dagger = s^\dagger \tilde{f} + \chi_{df}[d^\dagger \times \tilde{f}]^{(3)}. \tag{5}$$

The parameters of the $sdf$ IBM Hamiltonian ($\epsilon_d, \epsilon_f, \kappa_2, \chi_{dd}, \chi_{ff}, \kappa_3$, and $\chi_{df}$) are obtained, for each considered nucleus, by equating the SCMF $(\beta_2,\beta_3)$ deformation energy surface to the expectation value of the $sdf$ IBM Hamiltonian of Eq. (3) in the $sdf$-boson coherent state [24]. Since the $\hat{L}\cdot\hat{L}$ term does not contribute to the energy surface, the parameter $\alpha$ is determined separately in such a way that the cranking moment of inertia obtained in the boson coherent state [25] at the equilibrium minimum is equated to the corresponding Inglis-Belyaev moment of inertia obtained from the SCMF calculation [26]. Here the latter is increased by 30%, taking into account the well-known fact that the Inglis-Belyaev formula underestimates the empirical moments of inertia. The $sdf$ IBM parameters used in this study are listed in Table I. Almost the same values of the boson-core parameters are chosen as those in Ref. [16], except for the strength parameter $\alpha$. For a more detailed account of the mapping procedure in the $sdf$ IBM framework, the reader is referred to Refs. [15,16].

Since here only states with one unpaired fermion are considered for the description of the low-energy structure of the odd-even system, the single-particle Hamiltonian is simply

TABLE II. Single-particle energies $\epsilon_j$ and occupation probabilities $v_j^2$ of the odd neutron for the odd-mass isotopes $^{143,145,147}$Ba.

| | $^{143}$Ba | | $^{145}$Ba | | $^{147}$Ba | |
|---|---|---|---|---|---|---|
| | $\epsilon_j$ | $v_j^2$ | $\epsilon_j$ | $v_j^2$ | $\epsilon_j$ | $v_j^2$ |
| $3p_{1/2}$ | 3.374 | 0.012 | 3.421 | 0.018 | 3.461 | 0.023 |
| $3p_{3/2}$ | 2.732 | 0.017 | 2.797 | 0.024 | 2.856 | 0.033 |
| $2f_{5/2}$ | 2.464 | 0.032 | 2.537 | 0.045 | 2.605 | 0.059 |
| $2f_{7/2}$ | 0.443 | 0.173 | 0.552 | 0.243 | 0.652 | 0.319 |
| $1h_{9/2}$ | 0.000 | 0.319 | 0.000 | 0.441 | 0.000 | 0.556 |
| $1i_{13/2}$ | 3.333 | 0.020 | 3.378 | 0.028 | 3.417 | 0.036 |

given by $\hat{H}_F = \sum_j \epsilon_j [a_j^\dagger \tilde{a}_j]^{(0)}$, with $\epsilon_j$ the spherical single-particle energy for the orbital $j$. The energies are determined by the SCMF calculation constrained to zero deformation [9] and, together with the corresponding occupation probabilities, are listed in Table II. The fermion valence space for the nuclei $^{143,145,147}$Ba includes all single-particle levels in the neutron $N = 82-126$ major shell, that is, $3p_{1/2}$, $3p_{3/2}$, $1f_{5/2}$, $1f_{7/2}$, $1h_{9/2}$, and $1i_{13/2}$.

The boson-fermion interaction term $\hat{H}_{BF}$ consists of terms that represent the coupling of the odd neutron to the $sd$-boson space $\hat{H}_{BF}^{sd}$, to the $f$-boson space $\hat{H}_{BF}^{f}$, and to the combined $sdf$-boson space $\hat{H}_{BF}^{sdf}$:

$$\hat{H}_{BF} = \hat{H}_{BF}^{sd} + \hat{H}_{BF}^{f} + \hat{H}_{BF}^{sdf}. \tag{6}$$

The first term in Eq. (6) reads

$$\begin{aligned}\hat{H}_{BF}^{sd} = & \sum_{j_a j_b} \Gamma_{j_a j_b}^{sd} \hat{Q}_{sd} \cdot [a_{j_a}^\dagger \times \tilde{a}_{j_b}]^{(2)} \\ & + \sum_{j_a j_b j_c} \Lambda_{j_a j_b j_c}^{dd} : [[a_{j_a}^\dagger \times \tilde{d}]^{(j_c)} \times [d^\dagger \times \tilde{a}_{j_b}]^{(j_c)}]^{(0)} : \\ & + \sum_{j_a} A_{j_a}^{d} [a_{j_a}^\dagger \times \tilde{a}_{j_a}]^{(0)} \hat{n}_d, \end{aligned} \tag{7}$$

where the first, second, and third terms are referred to as (quadrupole) dynamical, exchange, and monopole terms, respectively [11,27]. $\hat{Q}_{sd}$ is the $sd$ part of the quadrupole operator in Eq. (4). In the following, single-particle orbitals are denoted by $j_a, j_b, j_c, \ldots$, while primed ones, such as $j_a', j_b', j_c', \ldots$, stand for those with opposite parity, unless otherwise specified. In a similar fashion, the following Hamiltonian is employed for the $f$-boson part:

$$\begin{aligned}\hat{H}_{BF}^{f} = & \sum_{j_a j_b} \Gamma_{j_a j_b}^{ff} \hat{Q}_{ff} \cdot [a_{j_a}^\dagger \times \tilde{a}_{j_b}]^{(2)} \\ & + \sum_{j_a j_b j_c'} \Lambda_{j_a j_b j_c'}^{ff} : [[a_{j_a}^\dagger \times \tilde{f}]^{(j_c')} \times [f^\dagger \times \tilde{a}_{j_b}]^{(j_c')}]^{(0)} : \\ & + \sum_{j_a} A_{j_a}^{f} [a_{j_a}^{+} \times \tilde{a}_{j_a}]^{(0)} \hat{n}_f, \end{aligned} \tag{8}$$

where $\hat{Q}_{ff} = \chi_{ff}[f^\dagger \times \tilde{f}]^{(2)}$, that is, the third term of the quadrupole operator in Eq. (4). Finally, $\hat{H}_{BF}^{sdf}$ in Eq. (6) reads

$$\begin{aligned}\hat{H}_{BF}^{sdf} = & \sum_{j_a j_b'} \Gamma_{j_a j_b'}^{sf} \hat{V}_3^\dagger \cdot [a_{j_a}^\dagger \times \tilde{a}_{j_b'}]^{(3)} \\ & + \sum_{j_a j_b' j_c} \Lambda_{j_a j_b' j_c}^{df} : [[a_{j_a}^\dagger \times \tilde{d}]^{(j_c)} \times [f^\dagger \times \tilde{a}_{j_b'}]^{(j_c)}]^{(0)} : \\ & + \text{H.c.}, \end{aligned} \tag{9}$$

where the first term denotes the dynamical octupole term.

It has been shown in Ref. [27] that, within the generalized seniority scheme, simple expressions in terms of occupation probabilities of the unpaired fermion can be derived for the coefficients of each term in $\hat{H}_{BF}^{sd}$ in Eq. (7):

$$\begin{aligned} A_j^d &= -A_0^d \sqrt{2j+1}, \\ \Gamma_{j_a j_b}^{sd} &= \Gamma_0^{sd} \gamma_{j_a j_b}^{(2)}, \\ \Lambda_{j_a j_b j_c}^{dd} &= -2\Lambda_0^{dd} \sqrt{\frac{5}{2j_c+1}} \beta_{j_a j_c}^{(2)} \beta_{j_b j_c}^{(2)}. \end{aligned} \tag{10}$$

Here we include the $f$-boson degree of freedom, and obtain similar expressions for the boson-fermion coupling constants in $\hat{H}_{BF}^{f}$ and $\hat{H}_{BF}^{sdf}$. For the $f$-boson part,

$$\begin{aligned} A_j^f &= -A_0^f \sqrt{2j+1}, \\ \Gamma_{j_a j_b}^{ff} &= \Gamma_0^{ff} \gamma_{j_a j_b}^{(2)}, \\ \Lambda_{j_a j_b j_c'}^{ff} &= -2\Lambda_0^{ff} \sqrt{\frac{7}{2j_c'+1}} \beta_{j_a j_c'}^{(3)} \beta_{j_b j_c'}^{(3)}, \end{aligned} \tag{11}$$

and for the $sdf$-boson terms,

$$\begin{aligned} \Gamma_{j_a j_b'}^{sf} &= \Gamma_0^{sf} \gamma_{j_a j_b'}^{(3)}, \\ \Lambda_{j_a j_b' j_c}^{df} &= -2\Lambda_0^{df} \sqrt{\frac{7}{2j_c+1}} \beta_{j_a j_c}^{(2)} \beta_{j_b' j_c}^{(3)}. \end{aligned} \tag{12}$$

Note that $\gamma_{ij}^{(\lambda)} = (u_i u_j - v_i v_j) q_{ij}^{(\lambda)}$ and $\beta_{ij}^{(\lambda)} = (u_i v_j + u_j v_i) q_{ij}^{(\lambda)}$, where $q_{ij}^{(\lambda)}$ represents the matrix element of fermion quadrupole ($\lambda = 2$) or octupole ($\lambda = 3$) operators in the single-particle basis.

By following the procedure of Ref. [9], the occupation probabilities $v_j^2$ of the odd particle in the spherical orbital $j$, which appear in Eqs. (10)–(12), are determined by the SCMF calculation constrained to zero deformation. The $v_j^2$ values used in the present study for the odd-mass nuclei $^{143,145,147}$Ba are listed in Table II.

There are altogether 14 strength parameters for the boson-fermion interaction that have to be adjusted to the spectroscopic data for the odd-mass Ba isotopes: six ($\Gamma_0^{sd}, \Gamma_0^{ff}, \Lambda_0^{dd}, \Lambda_0^{ff}, A_0^d$, and $A_0^f$) for each of the normal-parity $3p_{1/2,3/2}2f_{5/2,7/2}1h_{9/2}$ and the unique-parity $1i_{13/2}$ single-particle configurations, and two additional parameters $\Gamma_0^{sf}$ and $\Lambda_0^{df}$. Among the considered odd-mass Ba isotopes, more experimental information about low-lying states is available for $^{145}$Ba [13]. Thus our strategy is to first determine the parameters to reproduce several key features of low-energy spectroscopic data for $^{145}$Ba. Then, under the assumption that the parameters change gradually

TABLE III. Strength parameters of the boson-fermion interaction $\hat{H}_{BF}$ in Eq. (6) employed in the present calculation for the $^{143,145,147}$Ba nuclei (in MeV units). The numbers in the upper (lower) row for each nucleus correspond to the unique-parity (normal-parity) single-particle configurations.

| | $\Gamma_0^{sd}$ | $\Gamma_0^{ff}$ | $\Lambda_0^{sd}$ | $\Lambda_0^{ff}$ | $A_0^{d}$ | $A_0^{f}$ | $\Gamma_0^{sf}$ | $\Lambda_0^{df}$ |
|---|---|---|---|---|---|---|---|---|
| $^{143}$Ba | 1.40 | 1.20 | 1.0 | 0.0 | −0.75 | −0.75 | 0.75 | 0.0 |
| | 0.35 | 0.12 | 1.1 | 1.1 | −1.3 | −1.3 | | |
| $^{145}$Ba | 1.40 | 1.20 | 1.0 | 0.0 | −0.80 | 0.0 | 0.75 | 0.0 |
| | 0.40 | 0.13 | 1.0 | 0.30 | −1.0 | −0.15 | | |
| $^{147}$Ba | 1.40 | 1.20 | 1.0 | 0.0 | −0.85 | 0.0 | 0.75 | 0.0 |
| | 0.45 | 0.15 | 0.60 | 0.60 | −1.0 | −0.30 | | |

with nucleon number, we determine the parameters for the neighboring isotopes $^{143}$Ba and $^{147}$Ba. Experiments have suggested that the ground state of $^{145}$Ba is mostly characterized by quadrupole deformation, and there is no strong coupling with the octupole shape variable [13]. A similar scenario has been suggested for $^{143,147}$Ba [13] and, therefore, we determine the strength parameters for the quadrupole and octupole modes separately. The fitting protocol for $^{145}$Ba is as follows:

(1) The strength parameters for the quadrupole part $\hat{H}_{BF}^{sd}$ ($\Gamma_0^{sd}$, $\Lambda_0^{dd}$, and $A_0^{d}$) are determined to reproduce (i) the excitation spectra of the lowest band for each parity as well as (ii) the energy difference between the lowest states of each parity: $E(5/2_1^-)$ for negative parity, and $E(9/2_1^+)$ for positive parity.

(2) The strength parameters for the $f$-boson part $\hat{H}_{BF}^{f}$ ($\Gamma_0^{ff}$, $\Lambda_0^{ff}$, and $A_0^{f}$) are specifically relevant to those states that are built on $f$-boson configurations. They are determined to reproduce the excitation spectra of (i) the $11/2^+$ level at 670 keV (bandhead of the second-lowest positive-parity band) for the normal-parity $pfh$ configuration, as well as (ii) the $15/2^-$ level at 1226 keV for the unique-parity $1i_{13/2}$ configuration, both suggested as candidates for octupole states in Ref. [13].

(3) The term $\hat{H}_{BF}^{sdf}$ is expected to play a minor role in low-lying states of the considered odd-mass Ba nuclei and, consequently, their strength parameters $\Gamma_0^{sf}$ and $\Lambda_0^{df}$ are included only perturbatively. In the present study, a constant value is chosen for the former, while the latter is neglected as it makes little contribution to low-energy excitation spectra.

The adjusted strength parameters for the $^{143,145,147}$Ba nuclei are listed in Table III. Most of the parameters exhibit only a gradual variation with nucleon number. The corresponding $sdf$-IBFM Hamiltonian has been numerically diagonalized by using the computer code ARBMODEL [28].

Electromagnetic transition probabilities analyzed in the present work are the electric quadrupole ($E2$) and octupole ($E3$). The $E\lambda$ ($\lambda = 2,3$) operator is composed of both the boson and fermion contributions:

$$\hat{T}^{(E\lambda)} = \hat{T}_B^{(E\lambda)} + \hat{T}_F^{(E\lambda)}. \tag{13}$$

For the $E2$ operator, the bosonic part reads $\hat{T}_B^{(E2)} = e_B^{(2)}\hat{Q}$, with the quadrupole operator $\hat{Q}$ defined in Eq. (4), and the fermion $E2$ operator

$$\hat{T}_F^{(E2)} = -e_F^{(2)} \sum_{j_a j_b} \frac{1}{\sqrt{5}} \gamma_{j_a,j_b}^{(2)} [a_{j_a}^\dagger \times \tilde{a}_{j_b}]^{(2)}. \tag{14}$$

$e_B^{(2)}$ and $e_F^{(2)}$ denote bosonic and fermion $E2$ effective charges, respectively, and the values $e_B^{(2)} = 0.1108\, e\,\mathrm{b}$ and $e_F^{(2)} = 0.5\, e\,\mathrm{b}$ are used for all the considered Ba isotopes. $e_B^{(2)}$ has been determined to reproduce the experimental value [5] of the $B(E2; 2_1^+ \to 0_1^+)$ transition rate in the even-even nucleus $^{144}$Ba. Similarly, for the $E3$ transition operator, the bosonic part reads $\hat{T}^{(E3)} = e_B^{(3)}(\hat{V}_3^\dagger + \hat{V}_3)$, and the fermion part can be written, in analogy to the quadrupole one, as

$$\hat{T}_F^{(E3)} = -e_F^{(3)} \sum_{j_a j_b'} \frac{1}{\sqrt{7}} \gamma_{j_a,j_b'}^{(3)} [a_{j_a}^\dagger \times \tilde{a}_{j_b'}]^{(3)}. \tag{15}$$

The $E3$ boson effective charge of $e_B^{(3)} = 0.09\, e\,\mathrm{b}^{3/2}$ is taken from our previous calculation of the same even-even Ba nuclei [16], while the $E3$ fermion charge of $e_F^{(3)} = 0.5\, e\,\mathrm{b}^{3/2}$ is employed in the present calculation.

## III. RESULTS FOR THE EVEN-EVEN Ba ISOTOPES

We first briefly discuss the results obtained for the even-even nuclei $^{142,144,146}$Ba. Figure 1 depicts the axially symmetric

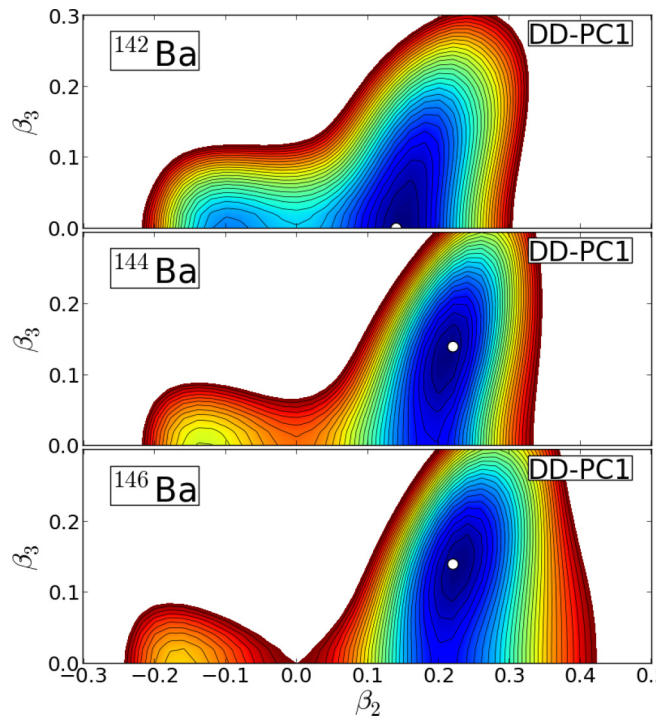


FIG. 1. SCMF $(\beta_2,\beta_3)$ deformation energy surfaces for $^{142,144,146}$Ba, obtained with the DD-PC1 nuclear functional [21] and a separable pairing force of finite range [22]. The energy difference between neighboring contours is 200 keV. Equilibrium minima are identified by open circles.

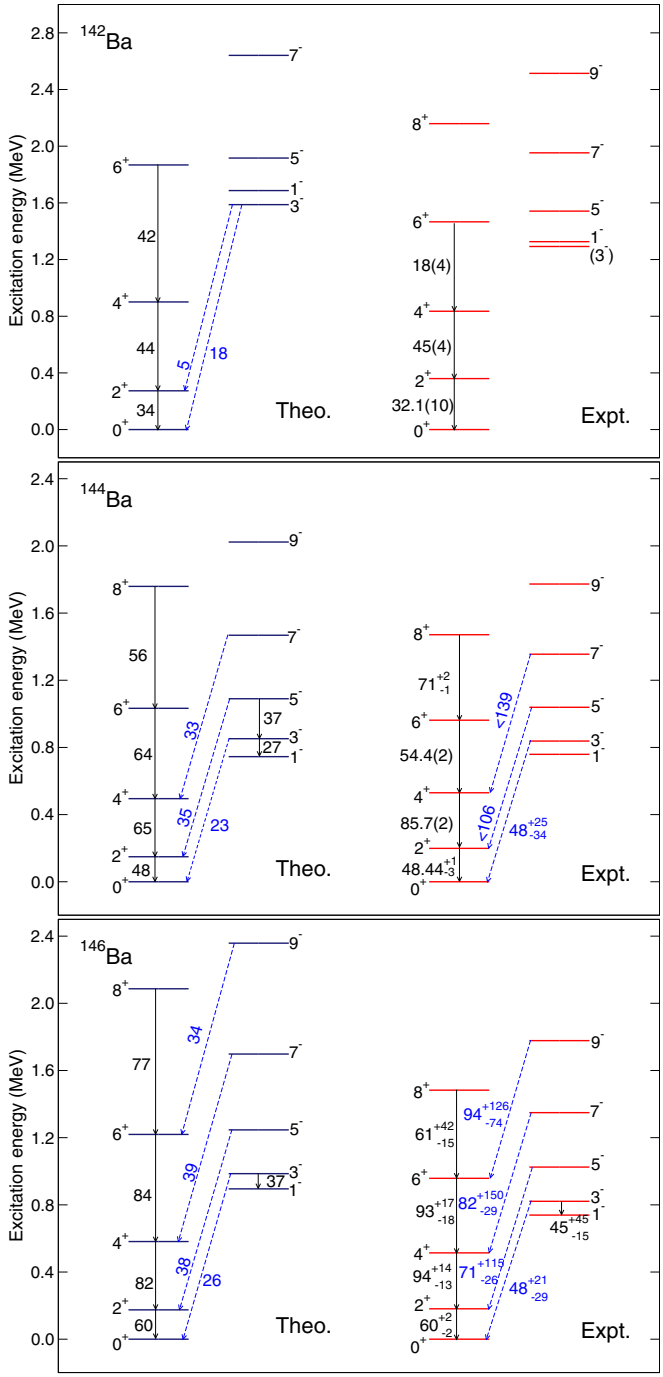


FIG. 2. Low-energy positive- and negative-parity spectra of the even-even boson core nuclei $^{142,144,146}$Ba. The $B(E2)$ (numbers along arrows within each band) and $B(E3)$ (interband, dashed arrows) values are given in Weisskopf units. Experimental values are taken from Refs. [29] ($^{142}$Ba), [5] ($^{144}$Ba), and [6] ($^{146}$Ba).

$(\beta_2,\beta_3)$ deformation energy surfaces calculated with the constrained relativistic Hartree-Bogoliubov method. For $^{142}$Ba the equilibrium minimum is found on the $\beta_3 = 0$ axis, indicating that it has a weakly deformed quadrupole shape. In $^{144,146}$Ba a minimum with nonzero $\beta_3$ deformation ($\beta \approx 0.1$) appears. The minimum is not very pronounced and is rather soft in the $\beta_3$ direction, suggesting the occurrence of octupole vibrational states in these nuclei.

The excitation spectra and transition rates for $^{142,144,146}$Ba are computed by diagonalizing the IBM Hamiltonian Eq. (3), determined from the SCMF $(\beta_2,\beta_3)$ deformation energy surface, in the $sdf$-boson basis. The low-energy level schemes for the $^{142,144,146}$Ba isotopes are displayed in Fig. 2. In general, the theoretical predictions are in good agreement with the experimental results [5,6,29], not only for the excitation energies but also for the $E2$ and $E3$ transition strengths. In the transition from the $^{142}$Ba to the $^{144}$Ba nucleus, in particular, we note the pronounced lowering of the the negative-parity band (cf. the corresponding SCMF deformation energy surface in Fig. 1). A rather large value $B(E3; 3^- \rightarrow 0^+)$ is predicted for all three even-even Ba nuclei, but still considerably smaller than the experimental values reported for $^{144,146}$Ba [5,6]. Note, however, the large uncertainty of the latter.

## IV. SPECTROSCOPIC PROPERTIES OF ODD-MASS Ba ISOTOPES

### A. Evolution of low-energy excitation spectra

In Figs. 3 and 4 the lowest energy negative- and positive-parity states for each spin of $^{143,145,147}$Ba are plotted as functions of the neutron number. Note that the spin and parity of the lowest $3/2^-$ state for $^{143}$Ba, the $3/2^-$, $11/2^+$, $15/2^+$, and $19/2^+$ states for $^{145}$Ba, and the $3/2^-$, $11/2^-$, $15/2^-$, $11/2^+$, $15/2^+$, and $19/2^+$ states have been assigned tentatively [12,13,29,30]. The excitation spectra obtained by the

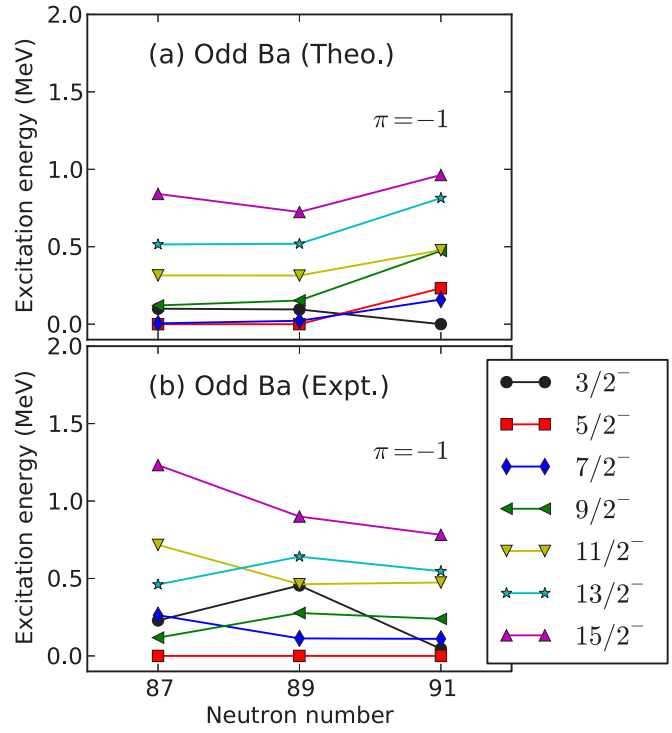


FIG. 3. Evolution of low-energy negative-parity levels of the odd-mass Ba isotopes as functions of the neutron number. Experimental excitation energies are taken from Refs. [12,13,30].

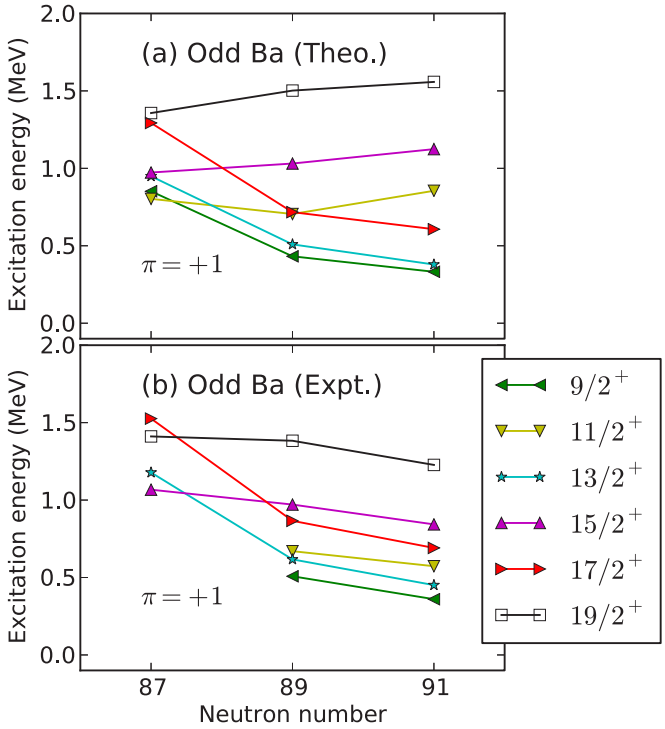


FIG. 4. Same as Fig. 3, but for the positive-parity levels.

diagonalization of the $sdf$-IBFM Hamiltonian reproduce the trend of the data, even though very little variation has been allowed for most of the strength parameters for the boson-fermion interaction (Table III). In $^{147}$Ba, however, experimentally the spin of the ground state is $J^\pi = 5/2^-$ [30], whereas in the present calculation it is $J^\pi = 3/2^-$. This state could be among the lowest in the data on $^{147}$Ba. A signature of shape transition is a rather rapid decrease of the $9/2^+$, $13/2^+$, and $17/2^+$ energy levels from $^{143}$Ba to $^{145}$Ba, and somewhat less steep from $^{145}$Ba to $^{147}$Ba. The empirical trend is

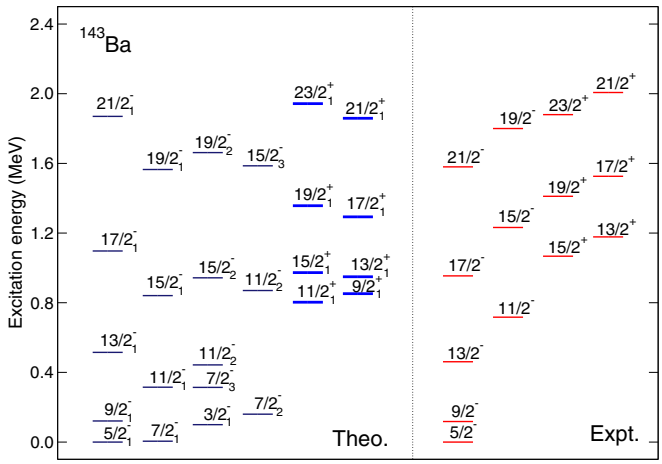


FIG. 5. Detailed comparison of the calculated and experimental low-energy positive- and negative-parity spectra of $^{143}$Ba. Those theoretical energy levels that are made of one $f$-boson configuration are drawn in bold and in color blue. Data are taken from Ref. [13].

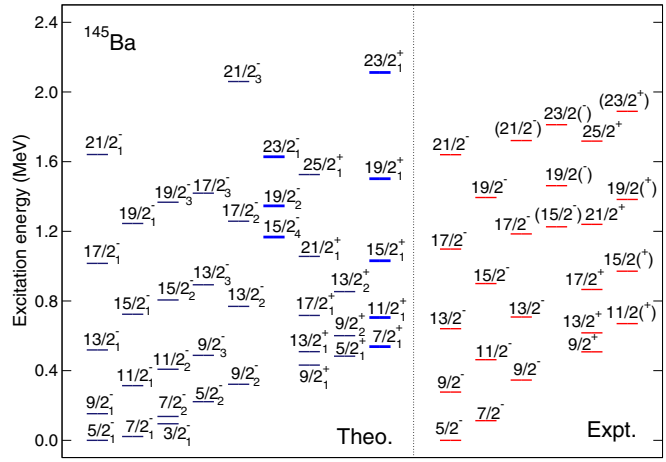


FIG. 6. Same as Fig. 5, but for the nucleus $^{145}$Ba. Experimental excitation energies are from Ref. [13].

nicely reproduced by the calculation, and this correlates with the fact that in the even-even systems, the nonzero octupole equilibrium deformation $\beta_3$ appears in the SCMF energy surface for $^{144}$Ba (Fig. 1). There are no distinct irregularities in the excitation spectra shown in Figs. 3 and 4.

### B. Detailed comparison of level schemes

Figures 5–7 display detailed comparisons between theoretical and experimental positive-parity and negative-parity low-lying bands in the odd-mass nuclei $^{143,145,147}$Ba. In organizing the theoretical level schemes, states are classified into bands according to the dominant $E2$ decay rates and the similarity in the composition of their IBFM wave functions. The labels in parentheses denote states that are assigned only tentatively in experiment. Also, only experimental states that are classified into bands are plotted in Figs. 5–7. Some experimental states that do not belong to these bands, for instance, the $3/2^-_1$ and $7/2^-_1$ states for $^{143}$Ba, are not included in Fig. 5, even though they are plotted in Fig. 3. In Tables V–IX we list the expectation values of the $f$-boson number operator $\langle \hat{n}_f \rangle$, as

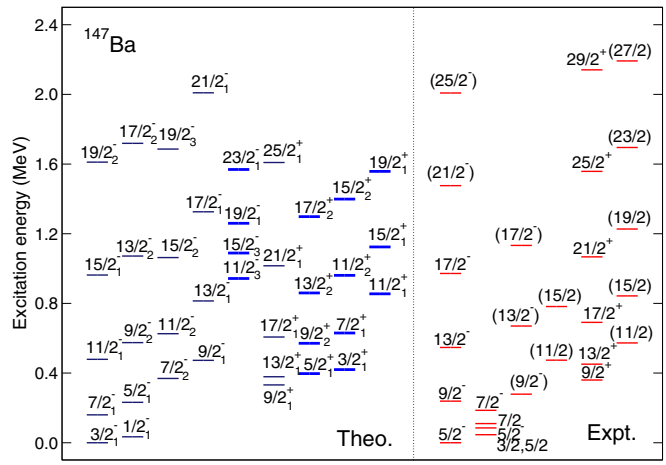


FIG. 7. Same as Fig. 5, but for $^{147}$Ba and with data from Ref. [30].

TABLE IV. Predicted $B(E2)$ and $B(E3)$ values (in Weisskopf units) for transitions among low-energy states of $^{143}$Ba.

| $B(E\lambda; J_i^\pi \to J_f^\pi)$ | Theory (W.u.) |
|---|---|
| $B(E2; 9/2_1^- \to 5/2_1^-)$ | 16 |
| $B(E2; 11/2_1^- \to 7/2_1^-)$ | 25 |
| $B(E2; 13/2_1^- \to 9/2_1^-)$ | 35 |
| $B(E2; 13/2_1^+ \to 9/2_1^+)$ | 21 |
| $B(E2; 15/2_1^+ \to 11/2_1^+)$ | 31 |
| $B(E2; 11/2_2^+ \to 7/2_1^+)$ | 4.2 |
| $B(E3; 11/2_1^+ \to 5/2_1^-)$ | 5.5 |
| $B(E3; 15/2_1^+ \to 9/2_1^-)$ | 11 |
| $B(E3; 13/2_1^+ \to 7/2_1^-)$ | 8.4 |
| $B(E3; 17/2_1^+ \to 11/2_1^-)$ | 13 |

well as the contribution of each single-particle component in the IBFM wave function of the band-head state of each band. The predicted $B(E2)$ and $B(E3)$ values are included in Tables VI–VIII. Note that presently data are not available for these quantities.

### *1.* $^{143}$Ba

For the even-even core nucleus $^{142}$Ba the SCMF $(\beta_2, \beta_3)$ deformation energy surface exhibits an equilibrium minimum at axial quadrupole deformation $\beta_2 \approx 0.14$ and octupole deformation $\beta_3 = 0$, and the corresponding spectra display negative-parity states at relatively high excitation energies compared to $^{144,146}$Ba. Hence, octupole deformation is expected to play a rather minor role in the odd-mass system $^{143}$Ba. Experimentally four bands, two of positive- and two negative-parity each, have been established in $^{143}$Ba [12]. The predicted level scheme shown in Fig. 5 reproduces nicely the lowest negative-parity ground-state band built on the $5/2_1^-$ state, as well as the energy of the $15/2_1^+$ state, which is the lowest positive-party state in experiment.

As shown in Table V, the present calculation does not predict the presence of octupole states (i.e., states that contain one or more $f$ bosons in their wave functions) in the vicinity of the ground state in $^{143}$Ba: all the negative-parity bands shown in Fig. 5 are composed mainly of the odd neutron in the $pfh$ orbitals coupled to the $sd$-boson space. On the other hand, the band built on the $11/2_1^+$ state is predicted to contain predominantly states with one $f$ boson, and similar for the $9/2_1^+$ band. From Table IV one notices several significant $B(E3)$ transition probabilities from the bands based on the $J^\pi = 9/2_1^+$ and $11/2_1^+$ states to the low-lying decoupled negative-parity band, e.g., $B(E3; 15/2_1^+ \to 9/2_1^-) = 11$ W.u. and $B(E3; 17/2_1^+ \to 11/2_1^-) = 13$ W.u.

TABLE V. Expectation value of the $f$-boson number operator $\langle \hat{n}_f \rangle$, and squares of the amplitudes (in percentage) of each spherical single-particle configuration in the IBFM wave functions of band-head states in $^{143}$Ba (cf. Fig. 5.)

| $J^\pi$ | $\langle \hat{n}_f \rangle$ | $3p_{1/2}$ | $3p_{3/2}$ | $2f_{5/2}$ | $2f_{7/2}$ | $1h_{9/2}$ | $1i_{13/2}$ |
|---|---|---|---|---|---|---|---|
| $5/2_1^-$ | 0.000 | 0 | 0 | 4 | 4 | 92 | 0 |
| $7/2_1^-$ | 0.000 | 0 | 0 | 2 | 5 | 93 | 0 |
| $3/2_1^-$ | 0.000 | 0 | 9 | 0 | 78 | 13 | 0 |
| $7/2_2^-$ | 0.001 | 0 | 9 | 0 | 80 | 11 | 0 |
| $11/2_1^+$ | 1.000 | 0 | 0 | 2 | 2 | 96 | 0 |
| $9/2_1^+$ | 1.000 | 0 | 0 | 2 | 3 | 95 | 0 |

TABLE VI. Same as Table IV, but for the $^{145}$Ba nucleus.

| $B(E\lambda; J_i^\pi \to J_f^\pi)$ | Theory (W.u.) |
|---|---|
| $B(E2; 7/2_1^- \to 5/2_1^-)$ | 23 |
| $B(E2; 9/2_1^- \to 5/2_1^-)$ | 10 |
| $B(E2; 11/2_1^- \to 7/2_1^-)$ | 23 |
| $B(E2; 13/2_1^- \to 9/2_1^-)$ | 38 |
| $B(E2; 11/2_1^+ \to 7/2_1^+)$ | 21 |
| $B(E2; 13/2_1^+ \to 9/2_1^+)$ | 75 |
| $B(E2; 15/2_1^+ \to 11/2_1^+)$ | 43 |
| $B(E2; 17/2_1^+ \to 13/2_1^+)$ | 78 |
| $B(E3; 11/2_1^+ \to 5/2_1^-)$ | 4.7 |
| $B(E3; 15/2_1^+ \to 9/2_1^-)$ | 15 |
| $B(E3; 13/2_1^+ \to 7/2_1^-)$ | 0.028 |
| $B(E3; 17/2_1^+ \to 11/2_1^-)$ | 0.59 |
| $B(E3; 15/2_1^- \to 9/2_1^+)$ | 0.00014 |
| $B(E3; 15/2_2^- \to 9/2_1^+)$ | 0.00078 |
| $B(E3; 15/2_4^- \to 9/2_1^+)$ | 25 |
| $B(E3; 19/2_2^- \to 13/2_1^+)$ | 31 |

### *2.* $^{145}$Ba

More experimental information is available on the isotope $^{145}$Ba and, as discussed in Sec. III, since the corresponding even-even boson core nucleus $^{144}$Ba exhibits an octupole-soft potential at the SCMF level (cf. Fig. 1), we also expect that octupole correlations play a more important role in the low-energy spectra of this nucleus. The calculated excitation spectrum is compared to the corresponding experimental bands in Fig. 6. As shown in Table VII, the lowest two negative-parity bands in $^{145}$Ba are built on the $5/2_1^-$ and $7/2_1^-$ states that are characterized by the coupling of the unpaired neutron in the $1h_{9/2}$ single-particle orbital to the $sd$-boson space. The lowest positive-parity state $9/2_1^+$ is described by the coupling of the $1i_{13/2}$ orbital to $sd$-boson states.

From Table VII it follows that the theoretical negative-parity band built on the $15/2_4^-$ state (calculated at 1167 keV) is dominated by the coupling of the $1i_{13/2}$ single-particle orbital to

TABLE VII. Same as Table V, but for $^{145}$Ba.

| $J^\pi$ | $\langle \hat{n}_f \rangle$ | $3p_{1/2}$ | $3p_{3/2}$ | $2f_{5/2}$ | $2f_{7/2}$ | $1h_{9/2}$ | $1i_{13/2}$ |
|---|---|---|---|---|---|---|---|
| $5/2_1^-$ | 0.000 | 0 | 0 | 5 | 3 | 92 | 0 |
| $7/2_1^-$ | 0.000 | 0 | 0 | 1 | 4 | 95 | 0 |
| $3/2_1^-$ | 0.005 | 3 | 17 | 1 | 67 | 11 | 0 |
| $5/2_2^-$ | 0.002 | 1 | 9 | 1 | 70 | 20 | 0 |
| $9/2_2^-$ | 0.000 | 0 | 1 | 2 | 8 | 89 | 0 |
| $15/2_4^-$ | 0.998 | 0 | 0 | 0 | 0 | 0 | 100 |
| $9/2_1^+$ | 0.000 | 0 | 0 | 0 | 0 | 0 | 100 |
| $5/2_1^+$ | 0.005 | 0 | 0 | 0 | 0 | 0 | 99 |
| $7/2_1^+$ | 1.000 | 0 | 0 | 1 | 4 | 95 | 0 |

TABLE VIII. Same as Table IV, but for the $^{147}$Ba nucleus.

| $B(E\lambda; J_i^\pi \to J_f^\pi)$ | Theory (W.u.) |
|---|---|
| $B(E2; 7/2_1^- \to 5/2_1^-)$ | 13 |
| $B(E2; 9/2_1^- \to 5/2_1^-)$ | 0.89 |
| $B(E2; 9/2_2^- \to 5/2_1^-)$ | 104 |
| $B(E2; 11/2_2^- \to 7/2_2^-)$ | 24 |
| $B(E2; 13/2_1^- \to 9/2_1^-)$ | 44 |
| $B(E2; 11/2_1^+ \to 7/2_1^+)$ | 0.17 |
| $B(E2; 13/2_1^+ \to 9/2_1^+)$ | 92 |
| $B(E2; 15/2_1^+ \to 11/2_1^+)$ | 48 |
| $B(E2; 17/2_1^+ \to 13/2_1^+)$ | 97 |
| $B(E3; 11/2_1^+ \to 5/2_1^-)$ | 0.037 |
| $B(E3; 11/2_2^+ \to 5/2_1^-)$ | 25 |
| $B(E3; 15/2_1^+ \to 9/2_1^-)$ | 15 |
| $B(E3; 15/2_3^- \to 9/2_1^+)$ | 29 |
| $B(E3; 19/2_1^- \to 13/2_1^+)$ | 38 |

states with one $f$ boson. Theoretically the $15/2_4^-$ state appears to be an octupole state and is located close to the experimental $15/2^-$ state found at 1226 keV [13]. Moreover, rather strong $E3$ transitions from the $J^\pi = 15/2_4^-$ band to the corresponding low-lying positive-parity bands are predicted: for instance, $B(E3; 15/2_4^- \to 9/2_1^+) = 25$ and $B(E3; 19/2_2^- \to 13/2_1^+) = 31$ (in W.u), comparable to the $B(E3; 3_1^- \to 0_1^+)$ value of 23 W.u. in the corresponding even-even core nucleus $^{144}$Ba (see Fig. 2). However, to verify model predictions, experimental information on the $B(E2)$ and $B(E3)$ values is needed.

For positive parity, the theoretical band built on the $7/2_1^+$ in $^{145}$Ba corresponds to the coupling of the $1h_{9/2}$ single-neutron configuration to states with one $f$ boson (cf. Table VII). The theoretical $11/2_1^+$ level, calculated at 705 keV, can be compared with the experimental $11/2^+$ state at 670 keV [13], which has been suggested as a candidate for an octupole state. Non-negligible $E3$ transition strength from the $7/2_1^+$ band to the negative-parity ground-state band is predicted in the present calculation: $B(E3; 11/2_1^+ \to 5/2_1^-) = 4.7$ and $B(E3; 15/2_1^+ \to 9/2_1^-) = 15$ (in W.u).

### 3. $^{147}$Ba

From the SCMF $(\beta_2, \beta_3)$ deformation energy surfaces of $^{144}$Ba and $^{146}$Ba (cf. Fig. 1) one expects rather similar low-energy excitation spectra in their odd-$N$ neighbors $^{145}$Ba and $^{147}$Ba, respectively. This is, to a certain extent, observed in the experimental spectra [30], even though the bands of $^{147}$Ba appear more compressed, as seen when comparing the data in Figs. 6 and 7. The ground-state spin $5/2^-$ has been identified for $^{147}$Ba, just as in the $^{143,145}$Ba neighbors [30]. This is, however, at variance within the present calculation, which predicts $3/2^-$ for the ground state. In fact, it is possible to reproduce the ground-state spin of $J = 5/2^-$ by playing with the parameters. In that case, however, one would have to choose an unrealistic value for the boson-fermion interaction strength, for instance, negative value for $\Gamma_0^{(sd)}$. The wrong sign implies that the single-particle energies and/or occupation probabilities used in the present calculation are not necessarily optimal. We then checked that decreasing the occupation probability for the $1h_{9/2}$ orbital, for instance, by 25%, allowed us to reproduce the correct level ordering of the ground state, but such an adjustment is not justified within the present framework and is beyond the scope of this paper. Nevertheless, one notices in Fig. 7 that a low-lying $J = 3/2$ level could be also present in experiment [30], i.e., among a set of levels close to the $J^\pi = 5/2^-$ ground state, even though its spin and parity have not been firmly established. Table IX also shows that the structure of the IBFM wave functions of the lowest lying states in $^{147}$Ba is different from those for $^{143,145}$Ba: they are dominated by the $1h_{9/2}$ configuration in $^{143,145}$Ba, whereas in $^{147}$Ba, the low-energy negative-parity states are characterized by the mixing of the $3p_{1/2,3/2}2f_{5/2,7/2}$ single-particle configurations.

TABLE IX. Same as Table V, but for $^{147}$Ba.

| $J^\pi$ | $\langle \hat{n}_f \rangle$ | $3p_{1/2}$ | $3p_{3/2}$ | $2f_{5/2}$ | $2f_{7/2}$ | $1h_{9/2}$ | $1i_{13/2}$ |
|---|---|---|---|---|---|---|---|
| $3/2_1^-$ | 0.002 | 14 | 38 | 9 | 39 | 0 | 0 |
| $1/2_1^-$ | 0.000 | 20 | 35 | 17 | 28 | 0 | 0 |
| $7/2_2^-$ | 0.000 | 0 | 0 | 0 | 2 | 98 | 0 |
| $9/2_1^-$ | 0.000 | 0 | 0 | 1 | 2 | 97 | 0 |
| $11/2_3^-$ | 0.996 | 0 | 0 | 0 | 0 | 0 | 100 |
| $9/2_1^+$ | 0.002 | 0 | 0 | 0 | 0 | 0 | 100 |
| $5/2_1^+$ | 0.950 | 10 | 31 | 8 | 45 | 0 | 6 |
| $3/2_1^+$ | 0.999 | 14 | 33 | 15 | 35 | 3 | 0 |
| $11/2_1^+$ | 1.000 | 0 | 0 | 1 | 2 | 97 | 0 |

One also notices from Table IX that states in the lowest two bands, built on the $3/2_1^-$ and $1/2_1^-$ states, do not contain $f$-boson components in their wave functions. The negative-parity bands built on the $7/2_2^-$ and $9/2_1^-$ states predominantly correspond to the $1h_{9/2}$ configuration coupled with the $sd$-boson space, and again there is no octupole $f$-boson component in these bands. The calculation predicts the lowest negative-parity octupole band to be the one built on the $11/2_3^-$ state, and this band is connected by rather strong $E3$ transition to the ground-state band, e.g., $B(E3; 15/2_3^- \to 9/2_1^+) = 29$ W.u. The experimental band built on the $11/2$ state at 573 keV (with tentative assignment of positive parity) has been identified as a possible octupole structure [30]. This band can be compared to the theoretical sequence with the $11/2_1^+$ band head at excitation energy 855 keV, dominated by the $1h_{9/2}$ single-particle orbital coupled to the $sdf$-boson space.

## V. CONCLUSIONS

The role of octupole correlations and the relevant spectroscopic properties of neutron-rich odd-mass Ba isotopes have been analyzed in a theoretical framework based on nuclear density functional theory and the particle-core coupling scheme. In the particular method employed in the present study, the interacting-boson Hamiltonian that describes the even-even core nucleus, as well as the single-particle energies and occupation probabilities of an unpaired nucleon, are completely determined by constrained SCMF calculations for a given choice of the energy density functional and pairing interaction. Only the coupling constants for the boson-fermion interaction are adjusted to selected spectroscopic data for the low-lying states in the odd-mass systems.

In this work the $sdf$-IBFM framework has been implemented: the boson-core Hamiltonian involves both quadrupole and octupole boson degrees of freedom and is constructed fully microscopically by mapping the axially symmetric $(\beta_2,\beta_3)$ deformation energy surface obtained by a constrained relativistic Hartree-Bogoliubov SCMF calculation onto the expectation value of the Hamiltonian in the $sdf$-boson condensate state. In the odd-mass Ba nuclei considered here the role of octupole deformation is not very important for the lowest levels near the ground state, and the adjustment of the boson-fermion strength parameters is relatively straightforward, even though there are many terms in the corresponding Hamiltonian of Eq. (6).

The SCMF $(\beta_2,\beta_3)$ deformation energy surfaces for the even-even Ba nuclei exhibit a transition from a weakly deformed quadrupole shape of $^{142}$Ba to moderately quadrupole- and octupole-deformed shapes of $^{144,146}$Ba, characterized by $\beta_3$-soft potentials. The resulting $sdf$ IBM energy spectra display a signature of octupole collectivity in the pronounced E3 transitions between the low-lying negative-parity band and the ground-state band, in agreement with recent spectroscopic data [5,6]. The $sdf$-IBFM reproduces the experimental low-energy excitation spectra in the considered odd-mass Ba isotopes fairly well. In particular, the present calculation indicates that octupole correlations are not present in the lowest states of $^{143,145,147}$Ba nuclei: most of their low-lying positive- and negative-parity yrast bands are predominantly formed by coupling the odd-neutron orbitals to the $sd$ boson space. Octupole states have been identified at somewhat higher excitation energy; e.g., in $^{145}$Ba the bands built on the $15/2^-_4$ and $7/2^+_1$ states are characterized by the coupling of the odd neutron to the $sd+f$ boson space, and exhibit pronounced $E3$ transitions to the ground-state band. These results, especially for $^{145,147}$Ba, are consistent with the conclusion of recent experimental studies [13,30].

A particularly interesting case for a follow-up study is that of the spectroscopic properties of actinide nuclei, e.g., $^{224,225}$Ra, where signatures of stable octupole shapes have been suggested and identified experimentally, such as parity doublets, pronounced electric dipoles, and octupole transitions. The low-energy states of these actinide nuclei are much richer in structure compared to the present case, because the octupole correlations are expected to be as prominent as the quadrupole ones. A quantitative analysis of quadrupole and octupole degrees of freedom in odd-mass nuclei in this region certainly presents a challenging application of the method introduced in the present work.

## ACKNOWLEDGMENTS

Part of this work was completed during the visit of K.N. to the Institut für Kernphysik (IKP), University of Cologne. He acknowledges IKP Cologne and Jan Jolie for their kind hospitality and financial support. This work was supported in part by the Croatian Science Foundation project "Structure and Dynamics of Exotic Femtosystems" (IP-2014-09-9159) and the QuantiXLie Centre of Excellence, a project cofinanced by the Croatian Government and European Union through the European Regional Development Fund, the Competitiveness and Cohesion Operational Programme (KK.01.1.1.01).

[1] P. A. Butler and W. Nazarewicz, Rev. Mod. Phys. **68**, 349 (1996).
[2] W. C. Haxton and E. M. Henley, Phys. Rev. Lett. **51**, 1937 (1983).
[3] J. Dobaczewski and J. Engel, Phys. Rev. Lett. **94**, 232502 (2005).
[4] L. P. Gaffney, P. A. Butler, M. Scheck, A. B. Hayes, F. Wenander, M. Albers, B. Bastin, C. Bauer, A. Blazhev, S. Bönig, N. Bree, J. Cederkäll, T. Chupp, D. Cline, T. E. Cocolios, T. Davinson, H. D. Witte, J. Diriken, T. Grahn, A. Herzan, M. Huyse, D. G. Jenkins, D. T. Joss, N. Kesteloot, J. Konki, M. Kowalczyk, T. Krll, E. Kwan, R. Lutter, K. Moschner, P. Napiorkowski, J. Pakarinen, M. Pfeiffer, D. Radeck, P. Reiter, K. Reynders, S. V. Rigby, L. M. Robledo, M. Rudigier, S. Sambi, M. Seidlitz, B. Siebeck, T. Stora, P. Thoele, P. V. Duppen, M. J. Vermeulen, M. von Schmid, D. Voulot, N. Warr, K. Wimmer, K. Wrzosek-Lipska, C. Y. Wu, and M. Zielinska, Nature (London) **497**, 199 (2013).
[5] B. Bucher, S. Zhu, C. Y. Wu, R. V. F. Janssens, D. Cline, A. B. Hayes, M. Albers, A. D. Ayangeakaa, P. A. Butler, C. M. Campbell, M. P. Carpenter, C. J. Chiara, J. A. Clark, H. L. Crawford, M. Cromaz, H. M. David, C. Dickerson, E. T. Gregor, J. Harker, C. R. Hoffman, B. P. Kay, F. G. Kondev, A. Korichi, T. Lauritsen, A. O. Macchiavelli, R. C. Pardo, A. Richard, M. A. Riley, G. Savard, M. Scheck, D. Seweryniak, M. K. Smith, R. Vondrasek, and A. Wiens, Phys. Rev. Lett. **116**, 112503 (2016).
[6] B. Bucher, S. Zhu, C. Y. Wu, R. V. F. Janssens, R. N. Bernard, L. M. Robledo, T. R. Rodríguez, D. Cline, A. B. Hayes, A. D. Ayangeakaa, M. Q. Buckner, C. M. Campbell, M. P. Carpenter, J. A. Clark, H. L. Crawford, H. M. David, C. Dickerson, J. Harker, C. R. Hoffman, B. P. Kay, F. G. Kondev, T. Lauritsen, A. O. Macchiavelli, R. C. Pardo, G. Savard, D. Seweryniak, and R. Vondrasek, Phys. Rev. Lett. **118**, 152504 (2017).
[7] R. H. Parker, M. R. Dietrich, M. R. Kalita, N. D. Lemke, K. G. Bailey, M. Bishof, J. P. Greene, R. J. Holt, W. Korsch, Z.-T. Lu, P. Mueller, T. P. O'Connor, and J. T. Singh, Phys. Rev. Lett. **114**, 233002 (2015).
[8] W. C. Griffith, M. D. Swallows, T. H. Loftus, M. V. Romalis, B. R. Heckel, and E. N. Fortson, Phys. Rev. Lett. **102**, 101601 (2009).
[9] K. Nomura, T. Nikšić, and D. Vretenar, Phys. Rev. C **93**, 054305 (2016).
[10] F. Iachello and A. Arima, *The Interacting Boson Model* (Cambridge University Press, Cambridge, England, 1987).
[11] F. Iachello and P. Van Isacker, *The Interacting Boson-Fermion Model* (Cambridge University Press, Cambridge, England, 1991).
[12] S. J. Zhu, J. H. Hamilton, A. V. Ramayya, E. F. Jones, J. K. Hwang, M. G. Wang, X. Q. Zhang, P. M. Gore, L. K. Peker, G. Drafta, B. R. S. Babu, W. C. Ma, G. L. Long, L. Y. Zhu, C. Y. Gan, L. M. Yang, M. Sakhaee, M. Li, J. K. Deng, T. N. Ginter, C. J. Beyer, J. Kormicki, J. D. Cole, R. Aryaeinejad, M. W. Drigert, J. O. Rasmussen, S. Asztalos, I. Y. Lee, A. O. Macchiavelli, S. Y. Chu, K. E. Gregorich, M. F. Mohar, G. M. Ter-Akopian, A. V. Daniel, Y. T. Oganessian, R. Donangelo, M. A. Stoyer,

R. W. Lougheed, K. J. Moody, J. F. Wild, S. G. Prussin, J. Kliman, and H. C. Griffin, Phys. Rev. C **60**, 051304 (1999).
[13] T. Rzaca-Urban, W. Urban, J. A. Pinston, G. S. Simpson, A. G. Smith, and I. Ahmad, Phys. Rev. C **86**, 044324 (2012).
[14] G. Leander, W. Nazarewicz, P. Olanders, I. Ragnarsson, and J. Dudek, Phys. Lett. B **152**, 284 (1985).
[15] K. Nomura, D. Vretenar, and B.-N. Lu, Phys. Rev. C **88**, 021303 (2013).
[16] K. Nomura, D. Vretenar, T. Nikšić, and B.-N. Lu, Phys. Rev. C **89**, 024312 (2014).
[17] D.-S. Chuu, S. T. Hsieh, and H. C. Chiang, Phys. Rev. C **47**, 183 (1993).
[18] C. Alonso, J. Arias, A. Frank, H. Sofia, S. Lenzi, and A. Vitturi, Nucl. Phys. A **586**, 100 (1995).
[19] A. K. Singh, G. Gangopadhyay, D. Banerjee, R. Bhattacharya, R. K. Bhowmik, S. Muralithar, R. P. Singh, A. Mukherjee, U. Datta Pramanik, A. Goswami, S. Chattopadhyay, S. Bhattacharya, B. Dasmalhapatra, and S. Sen, Phys. Rev. C **57**, 1617 (1998).
[20] D. Vretenar, A. Afanasjev, G. Lalazissis, and P. Ring, Phys. Rep. **409**, 101 (2005).
[21] T. Nikšić, D. Vretenar, and P. Ring, Phys. Rev. C **78**, 034318 (2008).
[22] Y. Tian, Z. Y. Ma, and P. Ring, Phys. Lett. B **676**, 44 (2009).
[23] A. F. Barfield, B. R. Barrett, J. L. Wood, and O. Scholten, Ann. Phys. (NY) **182**, 344 (1988).
[24] J. N. Ginocchio and M. W. Kirson, Nucl. Phys. A **350**, 31 (1980).
[25] H. Schaaser and D. M. Brink, Nucl. Phys. A **452**, 1 (1986).
[26] K. Nomura, T. Otsuka, N. Shimizu, and L. Guo, Phys. Rev. C **83**, 041302 (2011).
[27] O. Scholten, Prog. Part. Nucl. Phys. **14**, 189 (1985).
[28] S. Heinze, Computer program ARBMODEL, University of Cologne.
[29] Brookhaven National Nuclear Data Center, http://www.nndc.bnl.gov.
[30] T. Rząca-Urban, W. Urban, A. G. Smith, I. Ahmad, and A. Syntfeld-Każuch, Phys. Rev. C **87**, 031305(R) (2013).